

Towards a realization of Schwarzschild-(anti-)de Sitter spacetime as a particulate metamaterial

Tom G. Mackay¹

*School of Mathematics and Maxwell Institute for Mathematical Sciences
University of Edinburgh, Edinburgh EH9 3JZ, UK*

and

NanoMM — Nanoengineered Metamaterials Group

Department of Engineering Science and Mechanics

Pennsylvania State University, University Park, PA 16802-6812, USA

Akhlesh Lakhtakia²

NanoMM — Nanoengineered Metamaterials Group

Department of Engineering Science and Mechanics

Pennsylvania State University, University Park, PA 16802, USA

and

Materials Research Institute

Pennsylvania State University, University Park, PA 16802, USA

Abstract

While metamaterials offer the potential to realize Tamm mediums which represent vacuous spacetime subjected to gravitational fields, practical formulations for suitable metamaterials have not hitherto been developed. This matter is addressed by establishing a metamaterial formulation for the Tamm medium representing Schwarzschild-(anti-)de Sitter spacetime. Our formulation is remarkably simple and does not involve a complex nanostructure of the type that is often associated with metamaterials. Instead it is based on the homogenization of only isotropic dielectric and isotropic magnetic component mediums, which are distributed randomly as oriented spheroidal particles. Using the inverse Bruggeman homogenization formalism, we demonstrated that a wide range of constitutive parameter values for the Tamm medium may be accessed through varying the particle shape, volume fraction or relative permittivity and relative permeability of the component mediums. The presented formulation is appropriate for the regions of spacetime which lie outside the event horizon for Schwarzschild spacetime and inside the event horizon for de Sitter spacetime; there are no such restrictions for anti-de Sitter spacetime.

PACS numbers: 04.40.Nr, 98.80.-k, 41.20.Jb

Keywords: metamaterials, Bruggeman homogenization formalism, Tamm medium, Schwarzschild-(anti-)de Sitter spacetime

1 Introduction

Metamaterials constitute a notable class of engineered materials which offer opportunities for realizing such exotic phenomena as negative refraction and cloaking [1]. Furthermore, metamaterials offer unique op-

¹E-mail: T.Mackay@ed.ac.uk

²E-mail: akhlesh@psu.edu

portunities to investigate general relativistic scenarios [2]. This arises from the formal analogy that exists between light propagation in vacuum curved spacetime and propagation in a certain nonhomogeneous anisotropic or bianisotropic medium, known as a Tamm medium [3, 4, 5]. Lately, theoretical metamaterial-based analogs of black holes [6], de Sitter spacetime [7, 8], strings [9] including cosmic strings [10], and wormholes [11], for examples, have been proposed. Crucially, these spacetimes are amenable to representation by metamaterials because their metrics are time-independent.

While metamaterials may in principle be exploited to construct analogs of curved spacetime, concrete details of how this can be achieved in practice are conspicuously absent from the literature. A noteworthy exception is a recent description of a metamaterial representation of an artificial electromagnetic black hole [12], based upon the homogenization of simple components. However, the two-dimensional black hole considered is not astrophysical. In the following sections we develop a metamaterial formulation for a rather more complex curved spacetime scenario, which includes the Schwarzschild black hole and (anti-)de Sitter spacetime as specializations. Our formulation — which is remarkable for its simplicity — relies on the homogenization of isotropic dielectric and isotropic magnetic component mediums, which are distributed randomly as oriented spheroidal particles.

As regards notation, 3-vectors are underlined with the $\hat{}$ symbol denoting a unit vector, whereas 3×3 dyadics are double underlined with $\underline{\underline{I}}$ being the identity. The speed of light in vacuum in the absence of a gravitational field is $c_0 = 1/\sqrt{\epsilon_0\mu_0}$, where $\epsilon_0 = 8.854 \times 10^{-12}$ F m⁻¹ and $\mu_0 = 4\pi \times 10^{-12}$ H m⁻¹.

2 Tamm medium for Schwarzschild-(anti-)de Sitter spacetime

Static Schwarzschild-(anti-)de Sitter spacetime is conventionally represented by the line element [13, 14, 15]

$$d\tilde{s}^2 = \left(1 - \tilde{F}\right) d\tilde{t}^2 - \frac{1}{1 - \tilde{F}} d\tilde{r}^2 - \tilde{r}^2(d\tilde{\theta}^2 + \sin^2 \tilde{\theta} d\tilde{\phi}^2), \quad (1)$$

expressed in spherical coordinates with the adopted signature $(+, -, -, -)$. Herein the function

$$\tilde{F} = \frac{2GM}{c_0^2 \tilde{r}} + \frac{\Lambda \tilde{r}^2}{3c_0^2}, \quad (2)$$

with $M \geq 0$ being the mass of the corresponding Schwarzschild black hole, G the gravitational constant, and Λ the cosmological constant. The spacetime is called Schwarzschild–de Sitter spacetime if the cosmological constant Λ is positive; on the other hand, Schwarzschild–anti–de Sitter spacetime is characterized by $\Lambda < 0$. [16]. There are two noteworthy specializations, namely:

- (a) the $\Lambda = 0$ regime corresponds to Schwarzschild spacetime, and
- (b) the $M = 0$ regime corresponds to de Sitter or anti-de Sitter spacetime, according to whether Λ is positive or negative, respectively.

In terms of Cartesian coordinates $\tilde{x} = \tilde{r} \sin \tilde{\theta} \cos \tilde{\phi}$, $\tilde{y} = \tilde{r} \sin \tilde{\theta} \sin \tilde{\phi}$, and $\tilde{z} = \tilde{r} \cos \tilde{\theta}$, the line element (1) is represented by the metric $\tilde{g}_{\alpha\beta}$ as³

$$[\tilde{g}_{\alpha\beta}] = \begin{pmatrix} 1 - \tilde{F} & 0 & 0 & 0 \\ 0 & -1 - \frac{\tilde{F}\tilde{x}^2}{\tilde{r}^2(1 - \tilde{F})} & -\frac{\tilde{F}\tilde{x}\tilde{y}}{\tilde{r}^2(1 - \tilde{F})} & -\frac{\tilde{F}\tilde{x}\tilde{z}}{\tilde{r}^2(1 - \tilde{F})} \\ 0 & -\frac{\tilde{F}\tilde{x}\tilde{y}}{\tilde{r}^2(1 - \tilde{F})} & -1 - \frac{\tilde{F}\tilde{y}^2}{\tilde{r}^2(1 - \tilde{F})} & -\frac{\tilde{F}\tilde{y}\tilde{z}}{\tilde{r}^2(1 - \tilde{F})} \\ 0 & -\frac{\tilde{F}\tilde{x}\tilde{z}}{\tilde{r}^2(1 - \tilde{F})} & -\frac{\tilde{F}\tilde{y}\tilde{z}}{\tilde{r}^2(1 - \tilde{F})} & -1 - \frac{\tilde{F}\tilde{z}^2}{\tilde{r}^2(1 - \tilde{F})} \end{pmatrix}. \quad (3)$$

For our purposes here, it is more convenient to work with a diagonal metric. Therefore, we implement the (spatial) coordinate transformation represented by

$$\begin{pmatrix} t & x & y & z \end{pmatrix}^T = \mathbf{M} \cdot \begin{pmatrix} \tilde{t} & \tilde{x} & \tilde{y} & \tilde{z} \end{pmatrix}^T, \quad (4)$$

with the change of basis matrix

$$\mathbf{M} = \begin{pmatrix} 1 & 0 & 0 & 0 \\ 0 & \frac{\tilde{x}}{\tilde{r}} & -\frac{\tilde{z}}{\sqrt{\tilde{x}^2 + \tilde{z}^2}} & -\frac{\tilde{x}\tilde{y}}{\tilde{r}\sqrt{\tilde{x}^2 + \tilde{z}^2}} \\ 0 & \frac{\tilde{y}}{\tilde{r}} & 0 & \frac{\sqrt{\tilde{x}^2 + \tilde{z}^2}}{\tilde{r}} \\ 0 & \frac{\tilde{z}}{\tilde{r}} & \frac{\tilde{x}}{\sqrt{\tilde{x}^2 + \tilde{z}^2}} & -\frac{\tilde{y}\tilde{z}}{\tilde{r}\sqrt{\tilde{x}^2 + \tilde{z}^2}} \end{pmatrix}. \quad (5)$$

Since \mathbf{M} is an orthogonal matrix, we have $\tilde{r} \equiv r = \sqrt{x^2 + y^2 + z^2}$. With respect to this new coordinate system, the metric has the diagonal form

$$[g_{\alpha\beta}] \equiv \mathbf{M}^T \cdot [\tilde{g}_{\alpha\beta}] \cdot \mathbf{M} = \begin{pmatrix} 1 - \tilde{F} & 0 & 0 & 0 \\ 0 & \frac{1}{\tilde{F} - 1} & 0 & 0 \\ 0 & 0 & -1 & 0 \\ 0 & 0 & 0 & -1 \end{pmatrix}. \quad (6)$$

Following the noncovariant approach pioneered by Tamm [3, 4, 5], the electromagnetic response of vacuum in curved spacetime represented by the metric (6) may be described by the constitutive relations of an equivalent, instantaneously responding, medium (known as a Tamm medium) per [19]

$$\left. \begin{aligned} \underline{D} &= \epsilon_0 \underline{\underline{\gamma}} \cdot \underline{E} \\ \underline{B} &= \mu_0 \underline{\underline{\gamma}} \cdot \underline{H} \end{aligned} \right\}, \quad (7)$$

wherein SI units are implemented. Here, $\underline{\underline{\gamma}}$ is the 3×3 dyadic equivalent of the metric $[\gamma_{ab}]$ with components

$$\gamma_{ab} = -\frac{g^{ab}}{g_{00}}. \quad (8)$$

³Roman indexes take the values 1, 2 and 3; while Greek indexes take the values 0, 1, 2, and 3.

That is, the dyadic $\underline{\underline{\gamma}}$ has the uniaxial form

$$\underline{\underline{\gamma}} = \text{diag}(1, \gamma, \gamma), \quad (9)$$

where the scalar $\gamma = 1/(1 - \tilde{F})$.

In view of our quest to construct a Tamm medium with relative permittivity dyadic $\underline{\underline{\gamma}}$ and relative permeability dyadic $\underline{\underline{\gamma}}$, it is of interest to consider the spatial dependency of the parameter γ . In the case of Schwarzschild spacetime, γ with respect to r exhibits a singularity at $r = 2GM/c_0^2$, which corresponds to an event horizon. In the case of (anti-)de Sitter spacetime, γ with respect to r exhibits singularities at $r = \pm c_0\sqrt{3/\Lambda}$. Since $r \geq 0$, this corresponds to a single event horizon for de Sitter spacetime at $r = c_0\sqrt{3/\Lambda}$ and no event horizon for anti-de Sitter spacetime. Furthermore, $\gamma > 0$ outside the event horizon for Schwarzschild spacetime but inside the event horizon for de Sitter spacetime; and $\gamma > 0$ everywhere for anti-de Sitter spacetime. These features are illustrated in Fig. 1, wherein γ is plotted versus r for Schwarzschild and (anti-)de Sitter spacetimes for $M = |\Lambda| = 1.3$ using the normalizations $c_0 = G = 1$.

The situation for Schwarzschild-(anti-)de Sitter spacetime is rather more complicated, as is shown in Fig. 2 where γ is plotted versus r for Schwarzschild-(anti-)de Sitter spacetimes for $M = |\Lambda| = 0.3$ using the normalizations $c_0 = G = 1$. Now, for $r \geq 0$, γ with respect to r exhibits two singularities for Schwarzschild-de Sitter spacetime (and a third one for $r < 0$), while there is also one singularity for Schwarzschild-anti-de Sitter spacetime. Also, $\gamma > 0$ between the two singularities for Schwarzschild-de Sitter spacetime and outside the singularity for Schwarzschild-anti-de Sitter spacetime.

The distinction between the $\gamma > 0$ and $\gamma < 0$ regimes is of relevance when one considers the phenomenon of electromagnetic planewave propagation with negative phase velocity, which is pertinent to metamaterials which support negative refraction [17]. In fact, negative phase velocity can arise in the $\gamma < 0$ regime but not in the $\gamma > 0$ regime [18, 19]. The homogenization procedure presented in Sec. 3 is suitable for the $\gamma > 0$ regime only.

Finally in this section, we comment on a practical aspect of realizing the Tamm medium. In practice, the nonhomogeneous nature of the Tamm medium could be catered for by subdividing the space of interest into local neighbourhoods which are sufficiently small to be considered approximately homogeneous. The inverse homogenization procedures developed in Sec. 3 would then be applied locally. This piecewise homogeneous approach for the Tamm medium is documented in detail elsewhere [20].

3 Inverse Bruggeman formalism

The Tamm medium described by the constitutive relations (7) is a uniaxial dielectric-magnetic medium with identical relative permittivity and relative permeability dyadics. In order to construct such a medium, we turn to homogenization using as our basis the well-established Bruggeman formalism [21, 22].

Let us consider the homogenization of four component mediums, labelled a , b , c and d . Components a and b are isotropic dielectric mediums with relative permittivities ϵ_a and ϵ_b , and relative permeabilities $\mu_a = \mu_b = 1$. Components c and d are isotropic magnetic mediums with relative permeabilities μ_c and μ_d , and relative permittivities $\epsilon_c = \epsilon_d = 1$. The four component mediums are assumed to be randomly distributed, with respective volume fractions $f_a, f_b, f_c, f_d \in (0, 1)$ with $f_d = 1 - f_a - f_b - f_c$. Each component medium is composed of spheroidal particles which are small compared to the electromagnetic wavelengths under consideration. The axis of these spheroids for all four component mediums is taken to be aligned with the symmetry axis of $\underline{\underline{\gamma}}$, namely the \hat{x} axis. Thus, the surface of each spheroid relative to its centre is prescribed by the vector

$$r_s = \rho_\ell \underline{\underline{U}}_\ell \cdot \hat{x}, \quad (10)$$

where the positive-definite shape dyadic

$$\underline{\underline{U}}_\ell = \text{diag}(1, U_\ell, U_\ell), \quad (\ell = a, b, c, d), \quad (11)$$

the radial unit vector is $\hat{\underline{r}}$, and ρ_ℓ is a linear measure of size. Spheroids characterized by $U_\ell > 1$ are prolate whereas oblate spheroids are characterized by $U_\ell < 1$, and the degenerate spherical case corresponds to $U_\ell = 1$.

The Bruggeman formalism provides estimates of the relative permittivity dyadic $\underline{\underline{\epsilon}}_{Br} = \text{diag}(\epsilon_{Br}^x, \epsilon_{Br}, \epsilon_{Br})$ and the relative permeability dyadic $\underline{\underline{\mu}}_{Br} = \text{diag}(\mu_{Br}^x, \mu_{Br}, \mu_{Br})$ of the homogenized composite medium (HCM), as follows. Let us introduce the polarizability density dyadics

$$\left. \begin{aligned} \underline{\underline{a}}_\ell^\epsilon &= \left(\epsilon_\ell \underline{\underline{I}} - \underline{\underline{\epsilon}}_{Br} \right) \cdot \left[\underline{\underline{I}} + \underline{\underline{D}}_\ell^\epsilon \cdot \left(\epsilon_\ell \underline{\underline{I}} - \underline{\underline{\epsilon}}_{Br} \right) \right]^{-1} \\ \underline{\underline{a}}_\ell^\mu &= \left(\mu_\ell \underline{\underline{I}} - \underline{\underline{\mu}}_{Br} \right) \cdot \left[\underline{\underline{I}} + \underline{\underline{D}}_\ell^\mu \cdot \left(\mu_\ell \underline{\underline{I}} - \underline{\underline{\mu}}_{Br} \right) \right]^{-1} \end{aligned} \right\}, \quad (\ell = a, b, c, d). \quad (12)$$

The depolarization dyadics $\underline{\underline{D}}_\ell^{\epsilon, \mu}$ herein are given by [23, 24]

$$\underline{\underline{D}}_\ell^m = \text{diag}(D_\ell^{mx}, D_\ell^m, D_\ell^m), \quad (\ell = a, b, c, d; \quad m = \epsilon, \mu), \quad (13)$$

where the components

$$D_\ell^{mx} = \frac{1 - g(\sigma_\ell)}{m_{Br}(\sigma_\ell - 1)}, \quad (14)$$

$$D_\ell^m = \frac{1}{2m_{Br}U_\ell^2} \left(g(\sigma_\ell) - \frac{1 - g(\sigma_\ell)}{\sigma_\ell - 1} \right), \quad (15)$$

with the function

$$g(\sigma_\ell) = \begin{cases} \frac{1}{\sqrt{1 - \sigma_\ell}} \tanh^{-1}(\sqrt{1 - \sigma_\ell}), & 0 < \sigma_\ell < 1 \\ \frac{1}{\sqrt{\sigma_\ell - 1}} \tan^{-1}(\sqrt{\sigma_\ell - 1}), & \sigma_\ell > 1 \end{cases}, \quad (16)$$

and the dimensionless parameter $\sigma_\ell = U_\ell^2 m_{Br}^x / m_{Br}$. Parenthetically, these depolarization dyadics are only defined for the $\sigma_\ell > 0$ regime [23] — which corresponds the $\gamma > 0$ regime for the Tamm medium. According to the Bruggeman formalism, the constitutive parameters of the HCM are related to those of the component mediums by the dyadic equations [21, 22]

$$\left. \begin{aligned} \underline{\underline{A}}^\epsilon &= \underline{\underline{0}} \\ \underline{\underline{A}}^\mu &= \underline{\underline{0}} \end{aligned} \right\}, \quad (17)$$

where

$$\underline{\underline{A}}^m = f_a \underline{\underline{a}}_a^m + f_b \underline{\underline{a}}_b^m + f_c \underline{\underline{a}}_c^m + f_d \underline{\underline{a}}_d^m, \quad (m = \epsilon, \mu). \quad (18)$$

In fact, as the diagonal dyadics $\underline{\underline{A}}^m$ have the form $\text{diag}(A^{mx}, A^m, A^m)$, ($m = \epsilon, \mu$), the dyadic equations (17) contain only four independent scalar equations, which are coupled via the constitutive parameters for the HCM.

Conventionally, homogenization formalisms are applied in the forward sense, wherein the constitutive parameters of the HCM are estimated from a knowledge of the constitutive parameters of the component mediums. However, since our aim here is to find values of $\epsilon_{a,b}$, $\mu_{c,d}$, $f_{a,b,c}$ and $U_{a,b,c,d}$ such that the corresponding HCM coincides with the Tamm medium specified by the constitutive relations (7), we apply the Bruggeman formalism in its inverse sense. While formal expressions of the inverse Bruggeman formalism have been developed [25], these formal expressions can be ill-defined [26].⁴ In practice, it is more convenient to exploit direct numerical methods in order to implement the inverse formalism [28].

The following three distinct applications of the inverse Bruggeman formalism are considered, and illustrated using numerical examples in the next section. In each application, there are four scalar parameters to be determined.

⁴We note that certain constitutive parameter regimes have been found to be problematic for the inverse Bruggeman homogenization formalism [27], but these regimes do not overlap with the regimes considered here.

- (i) Assuming that the relative permittivities $\epsilon_{a,b}$ and relative permeabilities $\mu_{c,d}$ are known, and that $U_a = U_b = U_c = U_d = U$, we determine the common shape parameter U and the volume fractions f_a , f_b and f_c .
- (ii) Assuming that the relative permittivities $\epsilon_{a,b}$ and relative permeabilities $\mu_{c,d}$ are known, and that the volume fractions $f_{a,b,c}$ are fixed, we determine the shape parameters U_a , U_b , U_c and U_d .
- (iii) Assuming that the shape parameters $U_{a,b,c,d}$ and the volume fractions $f_{a,b,c}$ are fixed, we determine the relative permittivities $\epsilon_{a,b}$ and relative permeabilities $\mu_{c,d}$.

As a representative example, let us concentrate on the numerical implementation of application (i) — the numerical implementations for applications (ii) and (iii) are analogous. A modified Newton–Raphson technique [29, 30] may be implemented to extract the volume fractions $f_{a,b,c}$ and common shape factor U from eqs. (17). Using this technique, the solutions at step $k + 1$, namely $\{U^{(k+1)}, f_a^{(k+1)}, f_b^{(k+1)}, f_c^{(k+1)}\}$, are derived from those at step k , namely $\{U^{(k)}, f_a^{(k)}, f_b^{(k)}, f_c^{(k)}\}$, via the recursive scheme

$$\left. \begin{aligned} U^{(k+1)} &= U^{(k)} - \frac{A^{\epsilon x}(U^{(k)}, f_a^{(k)}, f_b^{(k)}, f_c^{(k)})}{\frac{\partial}{\partial U} A^{\epsilon x}(U^{(k)}, f_a^{(k)}, f_b^{(k)}, f_c^{(k)})} \\ f_a^{(k+1)} &= f_a^{(k)} - \frac{A^{\epsilon}(U^{(k+1)}, f_a^{(k)}, f_b^{(k)}, f_c^{(k)})}{\frac{\partial}{\partial f_a} A^{\epsilon}(U^{(k+1)}, f_a^{(k)}, f_b^{(k)}, f_c^{(k)})} \\ f_b^{(k+1)} &= f_b^{(k)} - \frac{A^{\mu x}(U^{(k+1)}, f_a^{(k+1)}, f_b^{(k)}, f_c^{(k)})}{\frac{\partial}{\partial f_b} A^{\mu x}(U^{(k+1)}, f_a^{(k+1)}, f_b^{(k)}, f_c^{(k)})} \\ f_c^{(k+1)} &= f_c^{(k)} - \frac{A^{\mu}(U^{(k+1)}, f_a^{(k+1)}, f_b^{(k+1)}, f_c^{(k)})}{\frac{\partial}{\partial f_c} A^{\mu}(U^{(k+1)}, f_a^{(k+1)}, f_b^{(k+1)}, f_c^{(k)})} \end{aligned} \right\}. \quad (19)$$

wherein the components of the dyadics $\underline{\underline{A}}^{\epsilon, \mu}$ are expressed as functions of the unknown parameters $\{U, f_a, f_b, f_c\}$.

For convergence of the scheme (19), it is vital that the initial estimates $\{U^{(0)}, f_a^{(0)}, f_b^{(0)}, f_c^{(0)}\}$ are chosen to be sufficiently close to the true solution. The forward Bruggeman formalism can be utilized in order to generate suitable initial estimates, as we now outline. Let $\{\epsilon_{Br}^x, \check{\epsilon}_{Br}, \check{\mu}_{Br}^x, \check{\mu}_{Br}\}$ denote the forward Bruggeman estimates of the HCM's relative permittivity and relative permeability parameters, computed for physically reasonable ranges of the parameters U and $f_{a,b,c}$, namely $U \in (U^+, U^-)$ and $f_{a,b,c} \in (f_{a,b,c}^+, f_{a,b,c}^-)$. Then:

- (1) Fix $f_a = (f_a^- + f_a^+)/2$, $f_b = (f_b^- + f_b^+)/2$, and $f_c = (f_c^- + f_c^+)/2$. For all values of $U \in (U^-, U^+)$, find the value U^\dagger for which the quantity

$$\Delta = \sqrt{(\epsilon_{Br}^x - 1)^2 + \left(\frac{\check{\epsilon}_{Br} - \gamma}{\gamma}\right)^2 + (\check{\mu}_{Br}^x - 1)^2 + \left(\frac{\check{\mu}_{Br} - \gamma}{\gamma}\right)^2} \quad (20)$$

is minimized.

- (2) Fix $U = U^\dagger$, $f_b = (f_b^- + f_b^+)/2$, and $f_c = (f_c^- + f_c^+)/2$. For all values of $f_a \in (f_a^-, f_a^+)$, find the value f_a^\dagger for which Δ is minimized.
- (3) Fix $U = U^\dagger$, $f_a = f_a^\dagger$, and $f_c = (f_c^- + f_c^+)/2$. For all values of $f_b \in (f_b^-, f_b^+)$, find the value f_b^\dagger for which Δ is minimized.
- (4) Fix $U = U^\dagger$, $f_a = f_a^\dagger$, and $f_b = f_b^\dagger$. For all values of $f_c \in (f_c^-, f_c^+)$, find the value f_c^\dagger for which Δ is minimized.

The steps (1)–(4) are repeated, using f_a^\dagger , f_b^\dagger , and f_c^\dagger as the fixed values of $f_{a,b,c}$ in step (i), f_b^\dagger and f_c^\dagger as the fixed values of $f_{b,c}$ in step (ii), and f_c^\dagger as the fixed value of f_c in step (iii), until Δ becomes sufficiently small.

In our numerical studies, we found that when $\Delta < 0.01$, the values of U^\dagger , f_a^\dagger , f_b^\dagger and f_c^\dagger provide suitable initial estimates for the modified Newton-Raphson scheme (19). In fact, we found that this technique of iteratively scanning the space of possible solutions could itself be used to find the inverse Bruggeman solutions, in some cases with a faster rate of convergence than the Newton-Raphson method and in a manner that is less sensitive to the initial estimates.

4 Numerical illustrations

We present numerical illustrations of the inverse homogenization applications (i)–(iii) described in Sec. 3. For each illustration, the parameter estimates for the component mediums are calculated as functions of γ . The ranges $\gamma > 1$ and $0 < \gamma < 1$ are considered — the $\gamma > 1$ range corresponds to Schwarzschild-de Sitter spacetime whereas the $0 < \gamma < 1$ corresponds to both Schwarzschild-de Sitter and Schwarzschild-anti-de Sitter spacetime, depending upon the magnitude of Λ . For all the numerical results presented in Figs. 3–5, the degree of convergence of the numerical schemes was $< 1\%$, and for most of the plotted points this value was $< 0.1\%$.

Let us begin with application (i). The common shape parameter U and the volume fractions $f_{a,b,c}$ are plotted versus γ in Fig. 3. For $0.8 < \gamma < 0.9$ we chose $\epsilon_a = 2$, $\epsilon_b = 0.1$, $\mu_c = 1.8$ and $\mu_d = 0.2$, while for $1 < \gamma < 2.9$ we chose $\epsilon_a = 8$, $\epsilon_b = 0.3$, $\mu_c = 7.4$ and $\mu_d = 0.4$. The common shape parameter increases sharply as γ increases, for both $0.8 < \gamma < 0.9$ and $1 < \gamma < 2.9$ ranges, while no particularly noteworthy trend is obvious from the volume fraction plots.

In Fig. 4, the shape parameters $U_{a,b,c,d}$ are presented as functions of γ for the application (ii). For $0.795 < \gamma < 0.805$ we chose $\epsilon_a = 2$, $\epsilon_b = 0.1$, $\mu_c = 1.8$ and $\mu_d = 0.2$ (as we chose for Fig. 3 for $0.8 < \gamma < 0.9$) and $f_{a,b} = 0.21$, $f_c = 0.3$, while for $1.9 < \gamma < 2.2$ we chose $\epsilon_a = 8$, $\epsilon_b = 0.3$, $\mu_c = 7.4$ and $\mu_d = 0.4$ (as we chose for Fig. 3 for $1 < \gamma < 2.9$) and $f_{a,b,c} = 0.25$. We see that $U_{a,c}$ decrease sharply as γ increases for $0.795 < \gamma < 0.805$, but increase sharply as γ increases for $1.9 < \gamma < 2.2$; the opposite trend is exhibited by $U_{b,d}$.

Finally, for application (iii), plots of the relative permittivities $\epsilon_{a,b}$ and relative permeabilities $\mu_{c,d}$ against γ are provided in Fig. 5. For $0.7 < \gamma < 1$ we chose the common shape parameter $U \equiv U_{a,b,c,d} = 0.01$ and the common volume fraction $f_{a,b,c} = 0.25$, while for $1.1 < \gamma < 2.9$ we chose the common shape parameter $U \equiv U_{a,b,c,d} = 5$ and the common volume fraction $f_{a,b,c} = 0.25$. For both $0.7 < \gamma < 1$ and $1.1 < \gamma < 2.9$ we found that the numerical schemes provide values of ϵ_a and μ_c which are almost the same, and values of ϵ_b and μ_d which are almost the same.

We close this section by remarking that the relative permittivities and relative permeabilities featured in Figs. 3–5 are neither unreasonably high nor unreasonably low from a physical perspective. Indeed, as regards the smallest values of $\epsilon_{a,b,c,d}$ and $\mu_{a,b,c,d}$ featured in Figs. 3–5, we note that materials with relative permittivities and relative permeabilities close to zero are currently subjects of intense investigation [31, 32, 33].

5 Closing remarks

By the homogenization of simple arrangements of four simple component mediums, the Tamm medium for Schwarzschild-(anti-)de Sitter spacetime may be constructed. The simplicity of this construction is especially noteworthy in view of the complex nanostructures which characterize many metamaterials designed for cloaking or negative refraction applications [1], for example. A wide range of constitutive parameter values for the Tamm medium can be accessed through varying the particle shape, volume fraction or relative permittivity and relative permeability of the component mediums. Thus, the inverse homogenization formulation delivers a practical strategy for designing an experimental analog for Schwarzschild-(anti-)de Sitter spacetime.

While the inverse homogenization scenario chosen for presentation in Sec. 3 was based on four component mediums, this formulation is not unique. Indeed, fewer components mediums may be used. For example, the Tamm medium for Schwarzschild-(anti-)de Sitter spacetime could similarly be conceptualized as arising from the homogenization of two component mediums, both of which being isotropic dielectric-magnetic mediums distributed as oriented spheroids. Alternatively, two component mediums could be used which were both uniaxial dielectric-magnetic mediums (with parallel symmetry axes) distributed as spherical particles. However, the four-component formulation presented herein incorporates very simple components, and accordingly offers a very large degree of freedom in choosing constitutive parameters.

Lastly, let us comment on the restriction of the inverse homogenization approach to those regions of spacetime which lie outside the event horizon for Schwarzschild spacetime and inside the event horizon for de Sitter spacetime (there being no such restrictions for anti-de Sitter spacetime). Equivalently, only Tamm mediums with positive-definite relative permittivity and relative permeability dyadics can be realized using this approach. The constitutive dyadics for the Tamm medium representing Schwarzschild-(anti-)de Sitter spacetime cannot possibly be negative definite but, as illustrated in Figs. 1 and 2, the indefinite scenario can arise (except in the case of anti-de Sitter spacetime). In principle, metamaterials with indefinite constitutive dyadics could be harnessed to construct a Tamm medium for the $\gamma < 0$ regime. Indeed, experimental studies of anisotropic dielectric [34] and anisotropic magnetic [35, 36] metamaterials with indefinite constitutive dyadics have already been reported. However, there are likely to be major practical difficulties in using such metamaterials to construct a $\gamma < 0$ Tamm medium: First, not only are the relative permittivity dyadic and the relative permeability dyadic both required to be indefinite (since the Tamm medium is an anisotropic dielectric-magnetic medium), but these two dyadics are required to be identical. Second, the metamaterials should be approximately nondissipative in order to faithfully represent the Tamm medium, but dissipation has proved to be a severe hindrance for many metamaterials. Finally, we add that conventional depolarization-dyadic-based homogenization techniques (as typified by the Bruggeman formalism) cannot be used to realize such metamaterials as nondissipative HCMs, since the indefinite nature of the constitutive dyadics renders the depolarization dyadics undefined [23]. This difficulty could be sidestepped by the incorporation of a small amount of dissipation [37], but at the cost of compromising the extent to which the resulting HCM represents the desired Tamm medium.

Acknowledgment: AL thanks the Charles Godfrey Binder Endowment at Penn State for partial financial support of his research activities.

References

- [1] T. J. Cui, D. R. Smith, and R. Liu, Eds., *Metamaterials: Theory, Design, and Applications* (Springer, New York, 2010).
- [2] I. I. Smolyaninov, *J. Opt.* **13**, 024004 (2011).
- [3] G. V. Skrotskii, *Soviet Phys.-Dokl.* **2**, 226 (1957).
- [4] J. Plébanski, *Phys. Rev.* **118**, 1396 (1960).
- [5] W. Schleich and M. O. Scully, in *New Trends in Atomic Physics*, Eds. G. Grynberg and R. Stora (Elsevier, Amsterdam, 1984), pp.995–1124.
- [6] I. I. Smolyaninov, *New J. Phys.* **5**, 147 (2003).
- [7] M. Li, R.-X. Miao, and Y. Pang, *Phys. Lett. B* **689**, 55 (2010).

- [8] M. Li, R.-X. Miao, and Y. Pang, Opt. Express **18**, 9026 (2010).
- [9] R.-X. Miao, R. Zheng, and M. Li, Phys. Lett. B **696**, 550 (2011).
- [10] T. G. Mackay and A. Lakhtakia, Phys. Lett. A **374**, 2305 (2010).
- [11] A. Greenleaf, Y. Kurylev, M. Lassas, and G. Uhlmann, SIAM Rev. **51**, 3 (2009).
- [12] W. Lu, J. Jin, Z. Lin, and H. Chen, J. Appl. Phys. **108**, 064517 (2010).
- [13] G. W. Gibbons and S. W. Hawking, Phys. Rev. D **15**, 2738 (1977).
- [14] J. Podolsky, Gen. Rel. Grav. **31**, 1703 (1999).
- [15] V. Cardoso and J. P. S. Lemos, Phys. Rev. D **64**, 084017 (2001).
- [16] H. Stephani, D. Kramer, M. MacCallum, C. Hoenselaers, and E. Herlt, *Exact Solutions of Einstein's Field Equations*, 2nd ed. (Cambridge University Press, Cambridge, UK, 2003), chapt. 8.
- [17] T. G. Mackay and A. Lakhtakia, Phys. Rev. B **79**, 235121 (2009).
- [18] T. G. Mackay, S. Setiawan, and A. Lakhtakia, Eur. Phys. J. C **41** (Supplement 1), 1 (2005).
- [19] T. G. Mackay, A. Lakhtakia, and S. Setiawan, Europhys. Lett. **71**, 925 (2005).
- [20] T. G. Mackay, A. Lakhtakia, and S. Setiawan, New J. Phys. **7**, 75 (2005).
- [21] W. S. Weiglhofer, A. Lakhtakia, and B. Michel, Microw. Opt. Technol. Lett. **15**, 263 (1997). Corrections: **22**, 221 (1999).
- [22] T. G. Mackay and A. Lakhtakia, *Electromagnetic Anisotropy and Bianisotropy: A Field Guide* (Word Scientific, Singapore, 2010), chap. 6.
- [23] B. Michel, Int. J. Appl. Electromagn. Mech. **8**, 219 (1997).
- [24] B. Michel and W. S. Weiglhofer, Arch. Elektron Übertrag. **51**, 219 (1997). Corrections: **52**, 310 (1998).
- [25] W. S. Weiglhofer, Microw. Opt. Technol. Lett. **28**, 421 (2001).
- [26] E. Cherkaev, Inverse Problems **17**, 1203 (2001).
- [27] S. S. Jamaian and T. G. Mackay, J. Nanophotonics **4**, 043510 (2010).
- [28] T. G. Mackay and A. Lakhtakia, J. Nanophotonics **4**, 041535 (2010).
- [29] P. A. Stark, *Introduction to Numerical Methods* (Macmillan, New York, 1970).
- [30] R. D. Kampia and A. Lakhtakia, J. Phys. D: Appl. Phys. **25**, 1390 (1992).
- [31] A. Alù, M. Silveirinha, A. Salandrino, and N. Engheta, Phys. Rev. B **75**, 155410 (2007).
- [32] G. Lovat, P. Burghignoli, F. Capolino, and D. R. Jackson, IET Microw. Antennas Propagat. **1**, 177 (2007).
- [33] M. N. Cia, M. Beruete, I. Campillo, and M. Sorolla, Phys Rev. B (accepted for publication).
- [34] H. Lee, Z. Liu, Y. Xiong, C. Sun, and X. Zhang, Opt. Express **15**, 15886 (2007).
- [35] A. B. Kozyrev, C. Qin, I. V. Shadrivov, Y. S. Kivshar, I. L. Chuang, and D. W. van der Weide, Opt. Express **15**, 11714 (2007).
- [36] J. Sun, L. Kang, R. Wang, L. Liu, L. Sun and J. Zhou, New J. Phys. **12**, 083020 (2010).
- [37] T. G. Mackay, A. Lakhtakia, and R. A. Depine, Microw. Opt. Technol. Lett. **48**, 363 (2006).

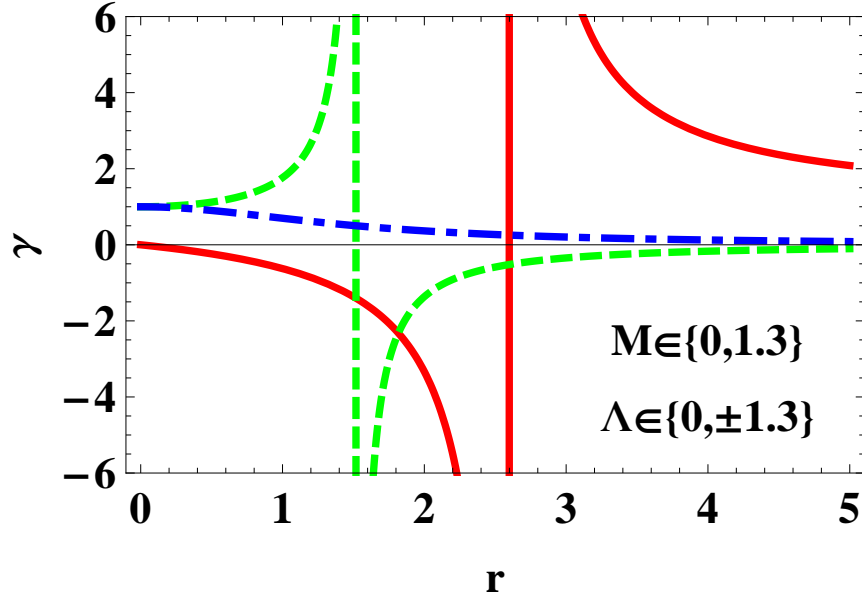


Figure 1: The parameter γ plotted versus r for Schwarzschild (solid, red), de Sitter (dashed, green) and anti-de Sitter (broken dashed, blue) spacetimes. Here $M \in \{0, 1.3\}$, $\Lambda \in \{0, \pm 1.3\}$ with the normalization $G = c_0 = 1$.

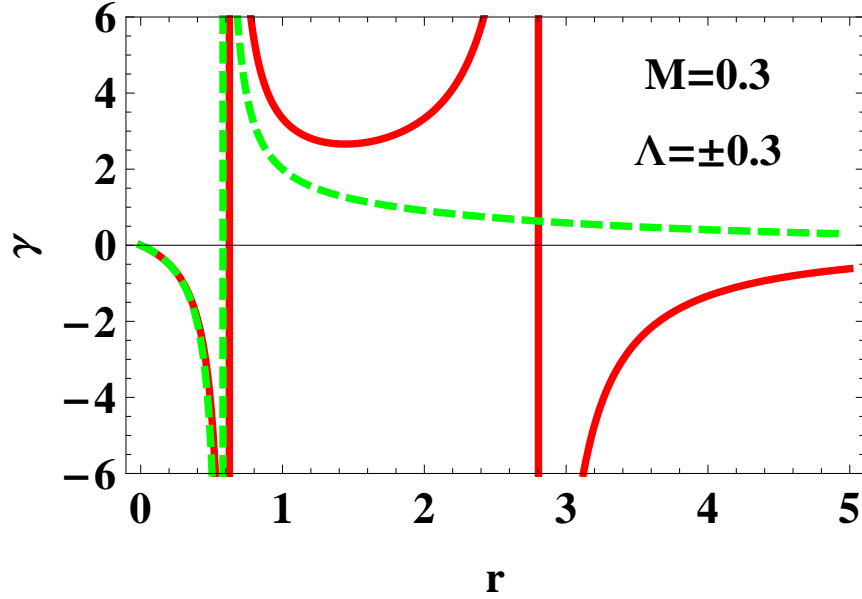


Figure 2: The parameter γ plotted versus r for Schwarzschild-de Sitter (solid, red) and Schwarzschild-anti-de Sitter (dashed, green) spacetimes. Here $M = 0.3$, $\Lambda = \pm 0.3$ with the normalization $G = c_0 = 1$.

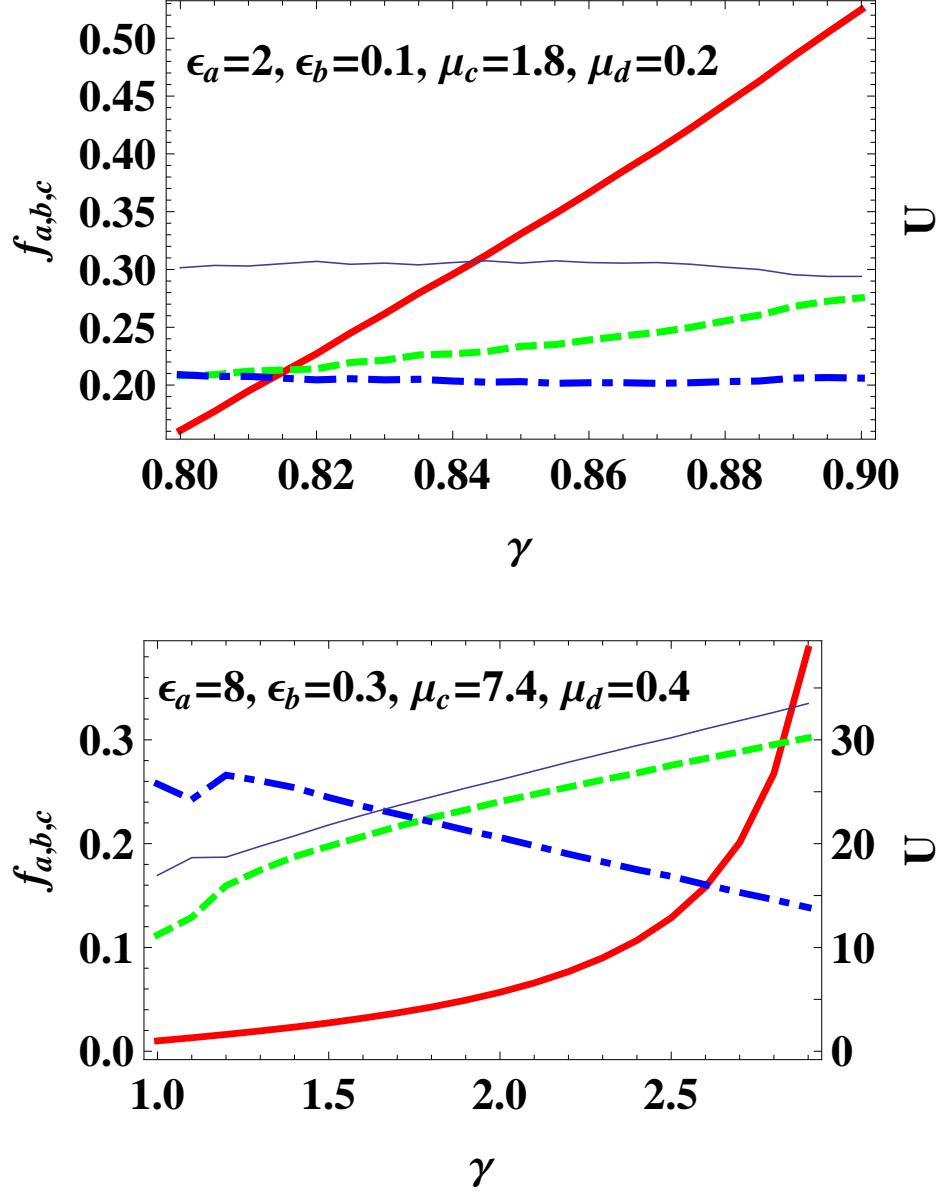


Figure 3: The common shape parameter U (thick solid, red) and volume fractions f_a (dashed, green), f_b (broken dashed, blue) and f_c (thin solid, blue) plotted versus γ . The relative permittivities $\epsilon_a = 2$, $\epsilon_b = 0.1$ and relative permeabilities $\mu_c = 1.8$, $\mu_d = 0.2$ for $0.8 < \gamma < 0.9$ (upper); and $\epsilon_a = 8$, $\epsilon_b = 0.3$, $\mu_c = 7.4$, $\mu_d = 0.4$ for $1 < \gamma < 2.9$ (lower).

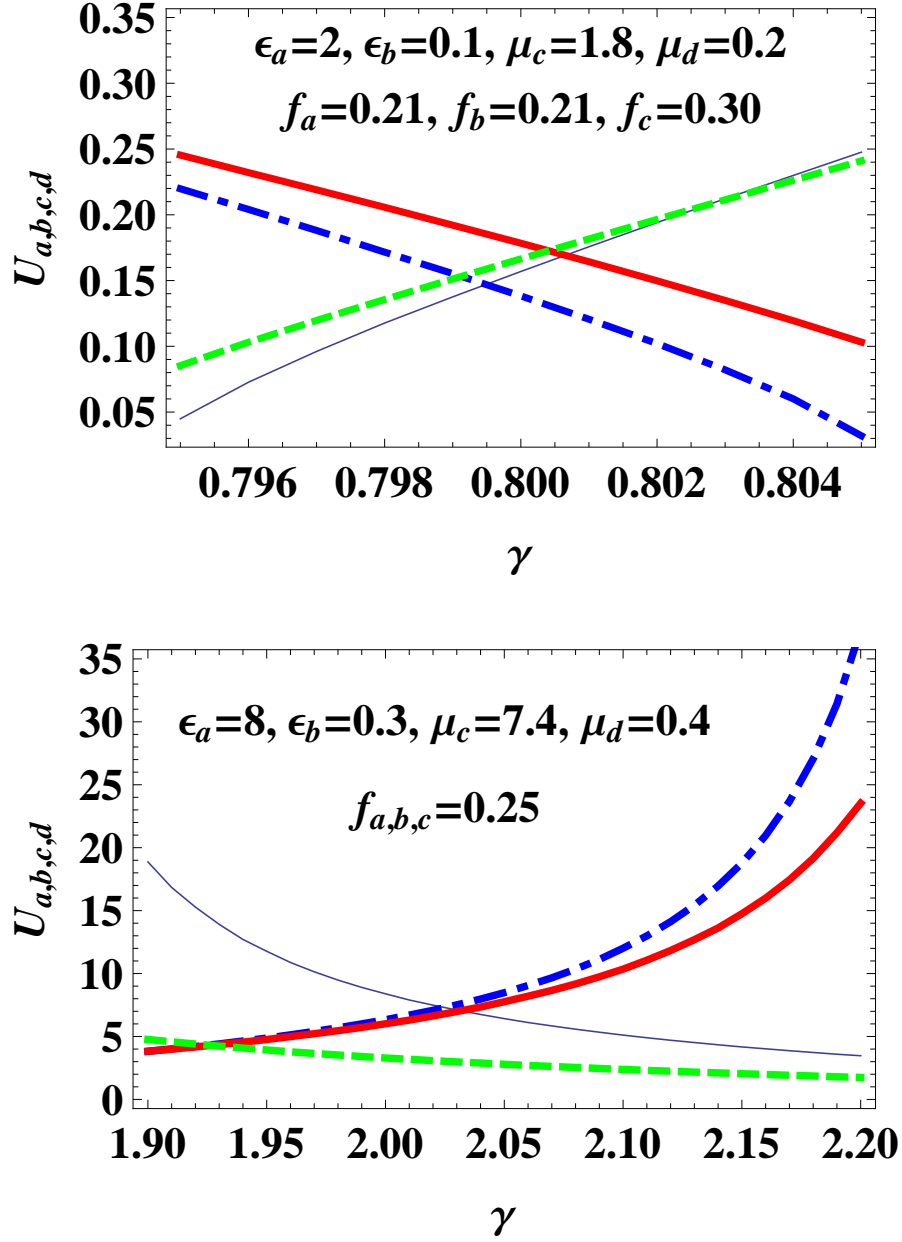


Figure 4: The shape parameters U_a (thick solid, red), U_b (dashed, green), U_c (broken dashed, blue) and U_d (thin solid, blue) plotted versus γ . The relative permittivities $\epsilon_a = 2$, $\epsilon_b = 0.1$ and relative permeabilities $\mu_c = 1.8$, $\mu_d = 0.2$ and volume fractions $f_a = 0.21$, $f_b = 0.21$ and $f_c = 0.3$ for $0.795 < \gamma < 0.805$ (upper); and $\epsilon_a = 8$, $\epsilon_b = 0.3$, $\mu_c = 7.4$, $\mu_d = 0.4$ and $f_{a,b,c,d} = 0.25$ for $1.9 < \gamma < 2.2$ (lower).

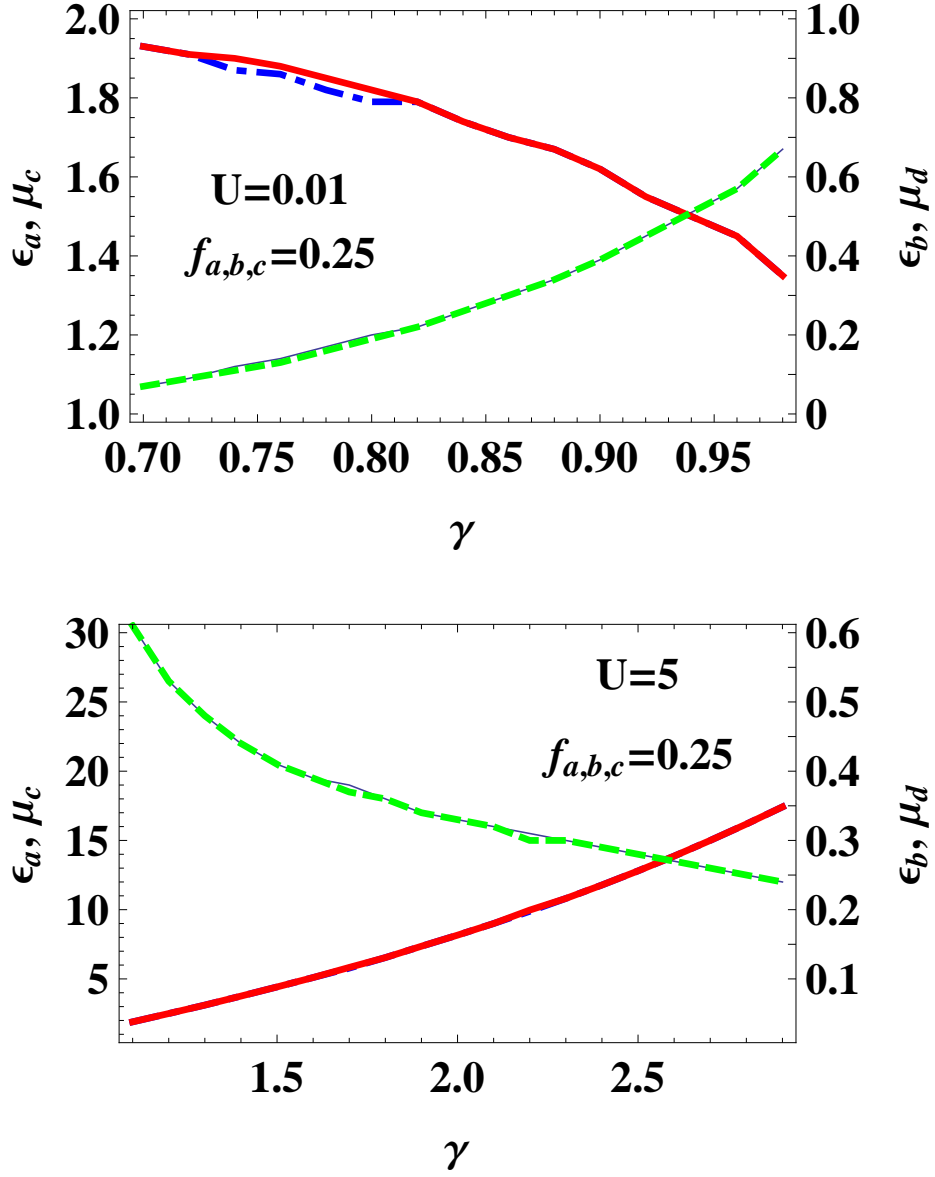


Figure 5: The relative permittivities ϵ_a (thick solid, red), ϵ_b (dashed, green) and relative permeabilities μ_c (broken dashed, blue), μ_d (thin solid, blue) plotted versus γ . The shape parameter $U = U_{a,b,c,d} = 0.01$ and volume fractions $f_{a,b,c} = 0.25$ for $0.7 < \gamma < 1$ (upper); and $U = U_{a,b,c,d} = 5$ and $f_{a,b,c} = 0.25$ for $1.1 < \gamma < 2.9$ (lower).